

Contents lists available at ScienceDirect

Case Studies in Construction Materials

journal homepage: www.elsevier.com/locate/cscm



Strengthening of RC flat slab-column connections against punching shear using engineered cementitious composites (ECC) with PE and hybrid steel/PE fibres: An experimental and theoretical study

Yanli Su^{a,b}, Chang Wu^{a,*}, Mingwen Xu^a, Xinru Wang^a, Chenhua Jin^c, Mingzhong Zhang^b

ARTICLE INFO

Keywords: Engineered cementitious composites (ECC) Flat slab system Punching shear Faillure mode Theoretical analysis

ABSTRACT

Engineered cementitious composite (ECC) exhibits excellent tensile properties and strainhardening behaviour, which has proven to be a potential material for addressing the brittle failure mode occurred in reinforced concrete (RC) flat systems. This study employs a systematic experimental and theoretical approach to investigate the improvement of punching shear behaviour in slab-column connections through the incorporation of ECC. Eight connections were designed accounting for the effects of ECC zone area, steel reinforcement ratio, and fibre type and dosage in ECC, which were subjected to concentric loading to investigate the load-bearing capacity, crack patterns, deformation characteristics and failure mechanisms. Experimental results indicate that all specimens ultimately failed through punching shear, while ECC-enhanced connections exhibited significantly improved ductility compared to conventional RC counterparts. ECC increased the first crack load and load-bearing capacity of connections by 18.58-33.31 % and 34.15-37.76 %, respectively. Yielding of the reinforcing bars was observed in all specimens, with higher reinforcement ratios and fibre dosages enhancing the yield load. Increasing the polyethylene (PE) fibre dosage in ECC from 1.0 % to 2.0 % led to a rise of the load capacity, deformation resistance and yield load. ECC with hybrid steel (0.5 %) and PE (1.5 %) fibres enhanced the structural stiffness but had a negligible effect on punching shear capacity when compared to ECC containing 2 % PE fibres. Punching shear failure surfaces consistently formed outside the ECC zone, effectively expanding the base perimeter of the shear cone and increasing the critical punching shear crack angle, which was considered to determine the critical section coefficient k. Applying the modified k to GB50010-2010 and DIN 1045-1 provisions gave accurate predictions of the punching shear strength for ECC-enhanced connections featuring critical sections of the punching shear cones outside the ECC zone.

E-mail address: changwu@seu.edu.cn (C. Wu).

a Key Laboratory of Concrete and Prestressed Concrete Structures of Ministry of Education, Southeast University, Nanjing 211189, China

^b Department of Civil, Environmental and Geomatic Engineering, University College London, London WC1E 6BT, United Kingdom

^c School of Architectural Engineering, Jinling Institute of Technology, Nanjing 211169, China

^{*} Corresponding author.

1. Introduction

Reinforced concrete (RC) flat slab system, characterised by the elimination of beams, enables efficient construction with typical column spacings of 4.5–6.0 m [1,2]. It has been widely adopted for different infrastructures such as buildings and underground parking garages because of the cost-effectiveness, enhanced spatial efficiency and simplified formwork requirements [3–5]. However, the absence of beam supports could induce concentrated transfer of bending moments and shear forces directly at slab-column connections. Such load transfer mechanism predisposes the connections to sudden punching shear failure, a brittle failure mode, which severely constrains the load and deformation capacities. More critically, such localised damage can trigger progressive collapse through sequential failure propagation within the slab system, posing significant safety risks [6–8].

The brittle punching shear failure observed in RC connection can be primarily attributed to the inherent brittleness of normal concrete [9]. Fibre reinforced concrete offers a viable strategy for enhancing the punching shear behaviour of these connections [10–13], since fibres can enhance the tensile properties and ductility of concrete. Engineered cementitious composites (ECC) have pseudo strain-hardening behaviour and excellent tensile properties [14,15]. ECC can achieve an ultimate tensile strain over 3 %, which is greater than that of normal concrete with a tensile strain of 0.1 % [16–18]. Incorporating ECC into structural members can delay steel reinforcement yielding while enhancing load-bearing capacity and ductility [19–24]. Recent studies have investigated the significance of ECC in enhancing the punching shear behaviour of concrete slabs [25–27]. In a previous study of the authors [25], small-scale (400 mm \times 400 mm \times 40 mm) ECC slabs were tested to characterize the effects of fibre dosage and span-to-depth ratio on the punching shear behaviour. It was found that ECC slabs exhibited an improved punching shear performance and a more ductile failure mode compared to normal concrete slabs. Compared to RC slab-column connections, reinforced ECC (RECC) specimens showed superior punching shear performance, characterized by a more ductile failure mode, progressive crack propagation, and greater energy dissipation [26,27]. Due to the potential economic constraints of constructing entire slabs with ECC in practical engineering applications, a proposed solution involves strategically utilising ECC specifically in the core areas of connections to enhance both punching shear capacity and ductility within flat slab systems.

Recent studies on punching shear behaviour of connections with ECC confirm the effectiveness of incorporating ECC in RC connections [28–34], in which vertical loads were directly applied to the slab-column connections and the effect of ECC zone area was systematically examined. It was observed that incorporating ECC can substantially enhance the punching shear resistance and overall ductility of the connection. The use of ECC shifts the failure mechanism from brittle punching shear to a more ductile shear-flexural mode. Expanding the ECC zone progressively improves the punching shear resistance until critical dimensions are reached, beyond which the strengthening effect declines markedly with further area extension. The balance between performance enhancement and economic cost should be considered for the optimisation of ECC zone size.

The existing studies [28–34] have provided valuable insights into the application of ECC in slab-column connections, while there still exist some limitations. Although preliminary investigations have confirmed that localised ECC zones can moderately enhance connection performance, the current understanding is predominantly limited to the isolated effects of ECC area. Research on the effects of reinforcement ratio, fibre type and fibre dosage in ECC on the punching shear response of flat slab system are not yet well understood. Given the relatively high cost of fibres, careful selection of fibre type and dosage is therefore essential for cost-effective engineering applications. Moreover, the punching shear failure surface in connections often extends beyond the ECC zone, the critical behavioural characteristics were not considered in current design codes, which rely on simplified concentric failure perimeters. The current experimental database remains insufficient to establish reliable model and parameters that accurately characterise the underlying mechanisms of punching shear resistance, and thus further experimental studies are needed.

This study investigates the punching shear behaviour of slab-column connections incorporating ECC with PE and hybrid steel/PE fibres in the core area. PE fibres provide exceptional tensile strain capacity and inherent corrosion resistance, while steel fibres contribute to enhanced stiffness. Eight connections were tested under concentrated loading to evaluate the effects of ECC zone area, steel reinforcement ratio, fibre type and fibre dosage in ECC on mechanical behaviour in terms of crack development, failure mode, critical loads and corresponding deflections. Importantly, as punching shear failure surfaces extended beyond the ECC zone, the critical shear perimeter was modified and integrated into existing design codes, providing a novel approach for predicting the punching shear strength of ECC-strengthened connections. This study offers both mechanistic insights and practical design guidance for the implementation of ECC in high-performance structural connections.

Table 1Mix proportions of ECC (kg/m³).

Mix ID	Cement	Fly ash	Sand	Water	Water reducer	PE fibre	Steel fibre
PE1-ECC	305.39	997.23	462.74	359.13	1.53	9.7	-
PE2-ECC						19.4	-
SP2-ECC						14.55	39.25

Note: Fibres are specified by volume fraction, whereas all other constituents are proportioned by mass ratio.

2. Experimental program

2.1. Materials and testing

ECC with varying fibre dosages (1 % and 2 % by volume) and fibre types (PE and steel), designated as PE1-ECC, PE2-ECC and SP2-ECC, were prepared. All mixes were prepared using P.O 42.5 cement, Class I fly ash, and quartz sand. Fine aggregate consisted of 70–120 mesh quartz sand. The mix proportions adopted in this study were listed in Table 1. For PE1-ECC and PE2-ECC, PE fibres were incorporated at dosages of 1 % and 2 %, respectively, while a hybrid of 0.5 % steel fibres and 1.5 % PE fibres by volume was adopted for SP2-ECC. The PE fibre is a monofilament with a smooth, glossy surface and is coated with silane coupling agents to enhance interfacial bonding with the cementitious matrix. The steel fibre is of a straight type, exhibiting a light grey metallic lustre, and has been galvanized to enhance both its corrosion resistance and interfacial adhesion with the matrix. The mechanical properties and images of the PE and steel fibres are presented in Table 2.

As per GB50010–2015 [35], six concrete cubes (150 mm cubes) were prepared and 28-day compressive strength was tested using a 3000 kN capacity universal hydraulic testing machine. The measured average compressive strength was 40.81 MPa, exhibiting a coefficient of variation (CoV) of 1.03 %. The 12-mm diameter HRB400 steel bars were adopted as internal reinforcement, the yield strength and ultimate tensile strength of which were 438 MPa (CoV = 2.61 %) and 630 MPa (CoV = 1.30 %), respectively.

Following JC/T 2416–2008 [36], dog-bone-shaped samples were used for tensile testing, while cubic specimens (side length of 100 mm) were prepared for compressive strength assessment of ECC. Fig. 1 shows the uniaxial tensile loading setup and typical tensile stress-strain curves of the ECC specimens. Six identical tensile and compressive specimens were tested and the average values of strengths of ECC are summarized in Table 3. The increase in fibre dosage from 1.0 % to 2.0 % had a negative effect on the compressive strength of ECC, consistent with the findings reported in Ref [32]. PE2-ECC exhibited an average compressive strength of 40.99 MPa, which was 9.47 % lower than that of PE1-ECC. Replacing 0.5 % of PE fibre with steel fibre in ECC had no significant impact on its compressive behaviour. In contrast, a fibre dosage from 1 % to 2 % enhanced the tensile performance, as evidenced by the PE2-ECC achieving a tensile strength of 5.05 MPa and an ultimate tensile strain of 2.68 %, representing increases of 33.95 % and 165.35 %, respectively, compared to PE1-ECC. Dense micro-cracks appeared in the tensile zone of PE-ECC with a fibre dosage of 2 %, while a few cracks were observed in the PE-ECC with a fibre dosage of 1 %. SP2-ECC also exhibited strain-hardening behaviour, with its tensile properties lower than those of PE2-ECC.

2.2. Specimen design

Eight slab-column connections were prepared, including two RC slab-column connections cast entirely with normal concrete and six RC connections enhanced with ECC. In the enhanced connections, ECC was cast within and around the column, while the reminding slab portions were made from normal concrete (Fig. 2b). Four variables were considered including ECC zone area, steel reinforcement ratio, fibre type and fibre dosage in ECC. Table 4 shows the details of all specimens. As per GB 50010–2010 [35], RC slab-column connections were reinforced with steel reinforcement ratios of 1.0 % and 1.5 % to prevent the slabs from experiencing a flexural failure mode. NC-1.0 referred to the RC connection specimen reinforced with a ratio of 1.0 %, while the other with 1.5 % was named as specimen NC-1.5. The remaining connections enhanced with ECC were named as EC-X-Y-Z, where EC denotes the reinforced concrete connections with ECC, X represents the steel reinforcement ratio, Y indicates the fibre types and Z is the side length of ECC zone. As reported in a previous study [28], the angle of punching shear failure surface of slabs ranged from 26.6° to 45°, accompanied by failure zone side lengths between 440 mm and 692 mm. In this study, the side lengths of ECC in connections were set as 440, 560 and 680 mm,

Table 2Properties and images of PE and steel fibres.

Fibre type	Density (kg/m³)	Length (mm)	Diameter (mm)	Tensile strength (MPa)	Elastic modulus (GPa)	Image
PE	0.97	12	0.024	3000	116	
Steel	7.80	13	0.220	2850	210	

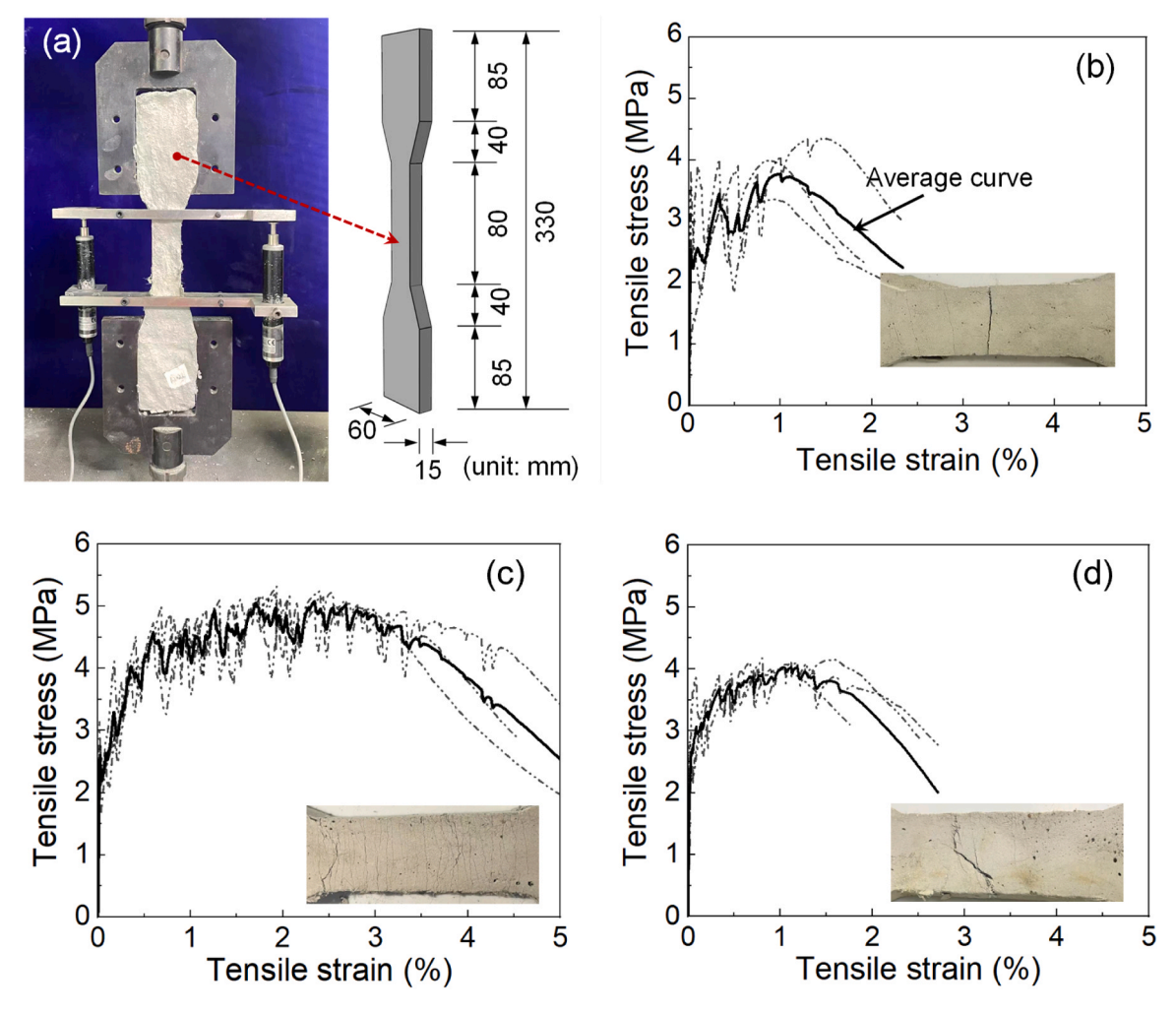


Fig. 1. Direct tensile test of ECC samples: (a) loading setup and sample dimension; and tensile stress-strain curves of (b) PE1-ECC, (c) PE2-ECC and (d) SP2-ECC.

Table 3Uniaxial tensile and compressive properties of ECC.

Mix ID	Tensile strength (MPa)	Tensile strain (%)	Compressive strength (MPa)
PE1-ECC	3.77 ± 0.19	1.01 ± 0.09	$\textbf{45.28} \pm \textbf{1.45}$
PE2-ECC	5.05 ± 0.11	2.68 ± 0.08	40.99 ± 1.02
SP2-ECC	4.05 ± 0.09	1.18 ± 0.03	43.40 ± 1.20

Note: The tensile strain refers to the axial strain recorded at the peak tensile stress (i.e., tensile strength) of the specimen.

respectively, corresponding to perimeters at distances equal to 1.0, 1.5 and 2.0 times the slab thickness from the column face. For instance, specimen EC-1.0-PE2-440 represented an RC connection enhanced with ECC (including 2 % PE fibre) and the side length of ECC zone was 440 mm.

Fig. 2 illustrates the dimensions and reinforcement configurations of RC connections with and without ECC. All slabs had identical dimensions, with on each side of 1400 mm and thickness of 120 mm. The lower column (60 mm tall) and upper column (120 mm tall) shared identical cross-sectional dimensions of 200 mm \times 200 mm. As per GB50010–2010 [35], the clear concrete cover was set as 20 mm for both slab and column. The steel reinforcement of the slabs consisted of 12-mm HRB400 rebars, arranged at 120-mm spacing in two orthogonal directions on the tensile side, achieving a flexural reinforcement ratio of 1.0 %. For connections with a 1.5 % reinforcement ratio, the rebar spacing was reduced to 80 mm. Longitudinal reinforcement comprised four rebars of 14 mm diameter in the column, and transverse reinforcement consisted of 8 mm diameter rebars arranged at 60 mm vertical spacing.

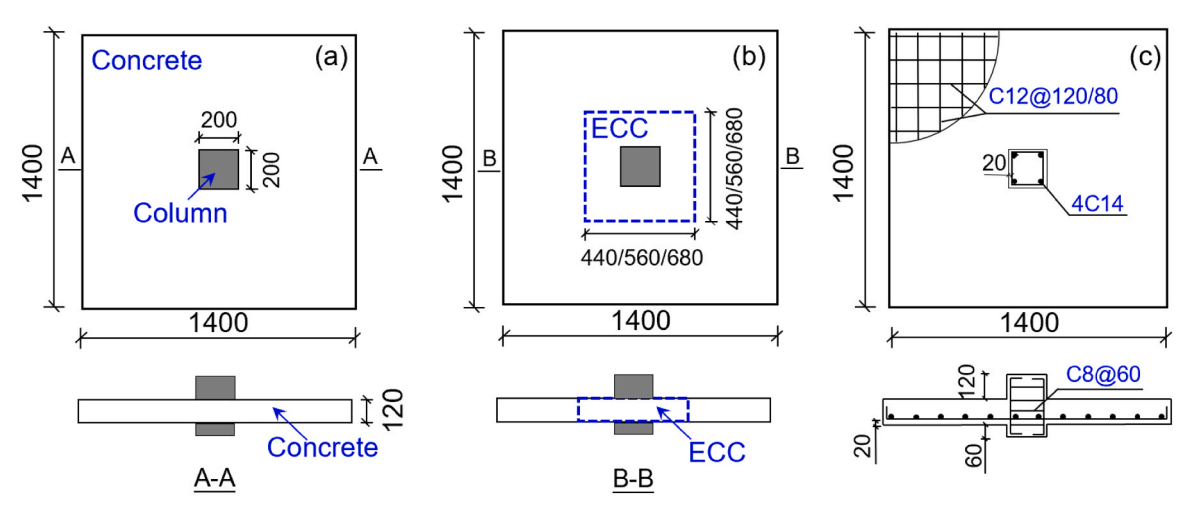


Fig. 2. Details of connections: (a) RC connection, (b) connections enhanced with ECC, and (c) reinforcement configurations (unit: mm).

Table 4 Details of the test specimens.

Specimen ID	Concrete type	Steel reinforcement ratio	Fibre type	Fibre dosage	Side length of ECC zone (mm)
NC-1.0	NC	1.0 %	-	-	-
NC-1.5	NC	1.5 %	-	-	-
EC-1.0-PE2-440	NC+ECC	1.0 %	PE	2 %	440
EC-1.0-PE2-560	NC+ECC	1.0 %	PE	2 %	560
EC-1.0-PE2-680	NC+ECC	1.0 %	PE	2 %	680
EC-1.0-SP2-440	NC+ECC	1.0 %	SF+PE	2 %	440
EC-1.0-PE1-440	NC+ECC	1.0 %	PE	1 %	440
EC-1.5-PE1-440	NC+ECC	1.5 %	PE	1 %	440

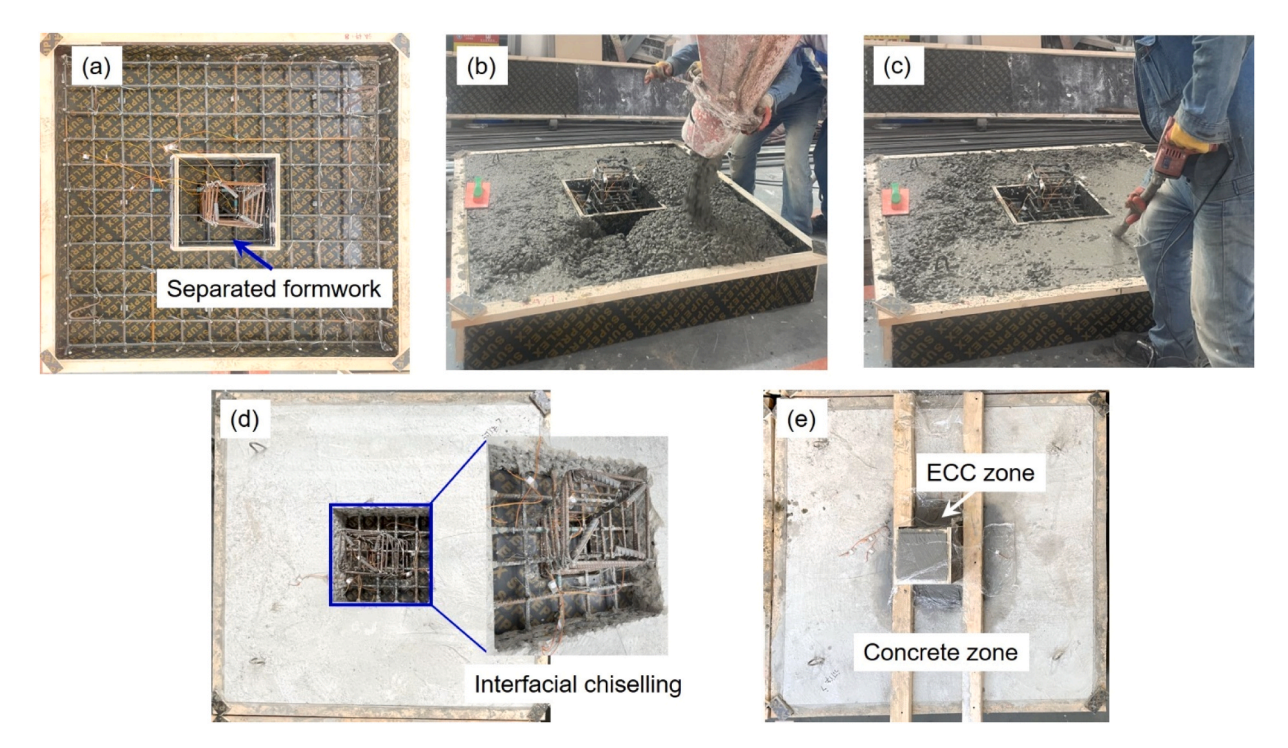


Fig. 3. Preparation of connections with ECC: (a) set up the formwork and install reinforcement stage, (b) pouring normal concrete, (c) vibrating concrete, (d) interfacial roughening by chiselling, and (e) hardened connections with ECC.

2.3. Specimen preparation

For specimens NC-1.0 and NC-1.5, wooden formwork was constructed to match the connection dimensions, and the steel reinforcement cage was subsequently placed inside. For the remaining specimens strengthened with ECC, a specialized formwork system was employed to demarcate the normal concrete and ECC zones (Fig. 3a). First, normal concrete was poured and internally vibrated to ensure proper compaction. The prepared connections were cured in the lab for 24 h. After curing, the separated formwork was removed, and the concrete surface was chiselled to enhance the interfacial bonding with ECC (Fig. 3d). ECC was then poured into the remaining areas of the slabs and columns, with dog-boned specimens and cubes cast simultaneously. Finally, all prepared specimens (Fig. 3e) were covered with plastic sheets for curing and tested at 28 d.

2.4. Test method

All specimens were tested using a 100 kN electronic universal testing machine, as shown in Fig. 4a. The loading rate of the specimen was 0.2 mm/min. The specimens were supported by a square steel frame with an internal side length of 1200 mm. The supporting frame was reinforced with vertical stiffeners to prevent deformation beneath the slab during testing. The test was terminated at the point where the load dropped to 80 % of the maximum load capacity reached.

A linear variable differential transformer (LVDT) with a 100 mm maximum range was mounted beneath the slab to measure central deflection and support settlement. Strain gauges were affixed to the centre of the longitudinal rebars to measure their strain. The layout of LVDTs and strain gauges on the rebars is illustrated in Figs. 4b and 4c.

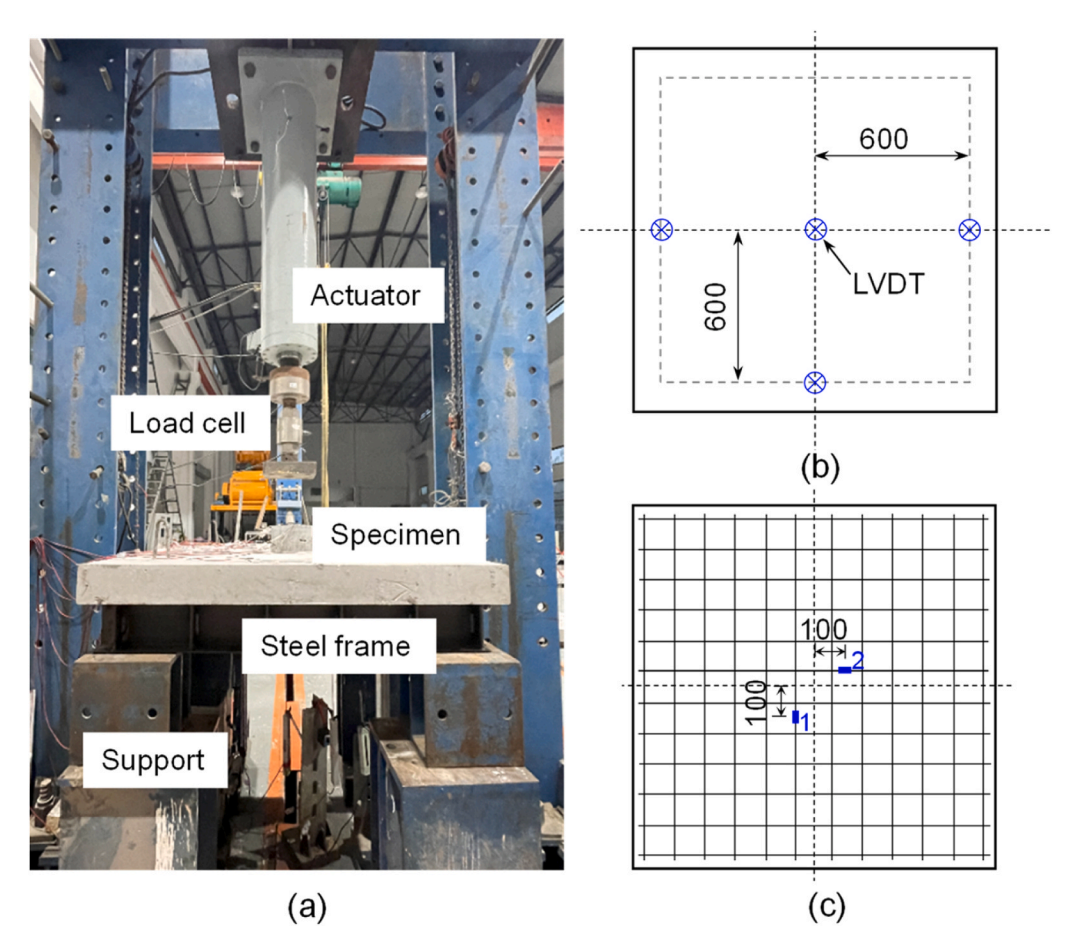


Fig. 4. Test setup and locations of measurement instrumentation: (a) test device, (b) arrangement of LVDT on the tensile side, and (c) strain gauges on steel rebars (unit: mm).

3. Experimental results and discussion

3.1. Crack development and failure patterns

3.1.1. Cracks on tensile side

Fig. 5 displays the crack development on the tensile side of two representative specimens NC-1.0 and EC-1.0-PE2–440 at different loading steps. Three critical stages, i.e. 80 kN, 120 kN and 200 kN, identified from the crack development of specimen NC-1.0 were selected to clearly illustrate the initiation and propagation of cracks with increasing applied load. Two distinct crack patterns can be observed, including radial flexural cracks and circumferential punching shear cracks. The radial flexural cracks were distributed perpendicular to the slab and column edges, and extending diagonally at an approximately 45° angle. Circumferential punching shear cracks were found around the column edge within the ECC zone during the loading process.

The crack development for specimens NC-1.0 and NC-1.5 looked similar. The first visible crack started from a column corner, followed by the formation of new radial cracks extending outward from the remaining column corners at approximately of 80 kN. As the load increased to 120 kN, circumferential cracks appeared around the column edges, while the number of flexural cracks increased, propagating towards the supporting edges. At 200 kN, the overall crack pattern essentially formed, comprising both flexural and shear cracks. Noticeable circumferential cracks were formed around the column edges, while flexural cracks developed across the entire slab.

For ECC-enhanced connections, the first radial crack was visible perpendicular to the column edge, followed by two symmetric cracks extending outward from all four sides of the column. At 120 kN, the initial flexural cracks grew towards the supporting edge, while the formation of new flexural cracks took place and circumferential cracks can be found within the ECC application zone. At 200 kN, there existed fine flexural cracks within the ECC application zone, and the circumferential cracks progressively grew.

Fig. 6 presents the final patterns on the tensile side of the connections, along with the punching shear failure zone outlined by dashed lines. No interfacial cracks formed between ECC and normal concrete, suggesting that ECC achieved a perfect bond with the normal concrete. Multiple fine cracks appeared within the ECC zone, as a result of the strain-hardening behaviour of ECC. The punching shear zone was expanded due to the incorporation of ECC. Specimen EC-1.0-PE2-440 with 2.0 % fibres had more fine cracks compared to specimen EC-1.0-PE1-440 with 1.0 % fibres due to the superior tensile cracking resistance of ECC with more fibres.

3.1.2. Cracks on saw-cut section

Fig. 7 presents the crack patterns on the saw-cut cross-section views of all specimens, indicating the internal crack development and failure mechanisms. The cutting sections were taken along the A–A and B–B planes indicated in Fig. 1. All specimens followed punching shear failure, featured by the formation of punching shear cones and the absence of flexural cracks. In specimens NC-1.0 and

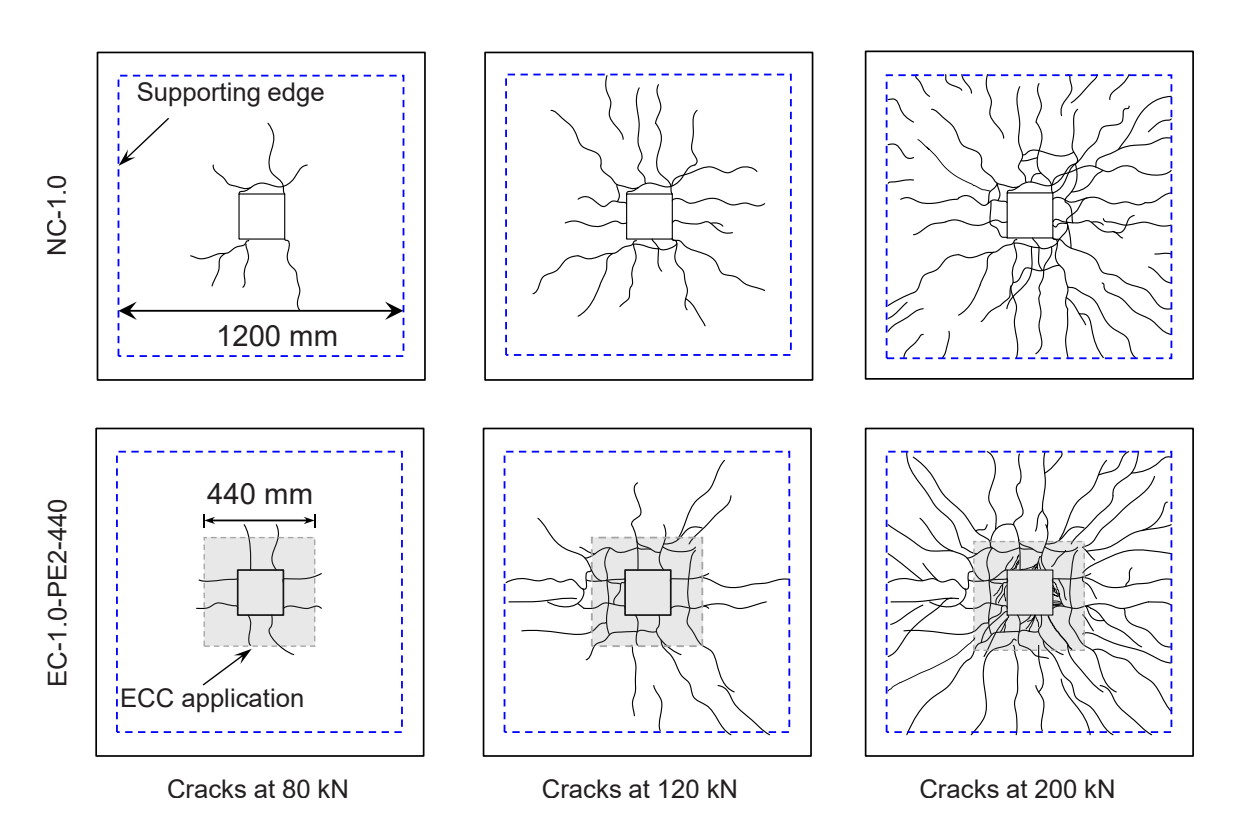


Fig. 5. Crack development of representative specimens at different loading levels.

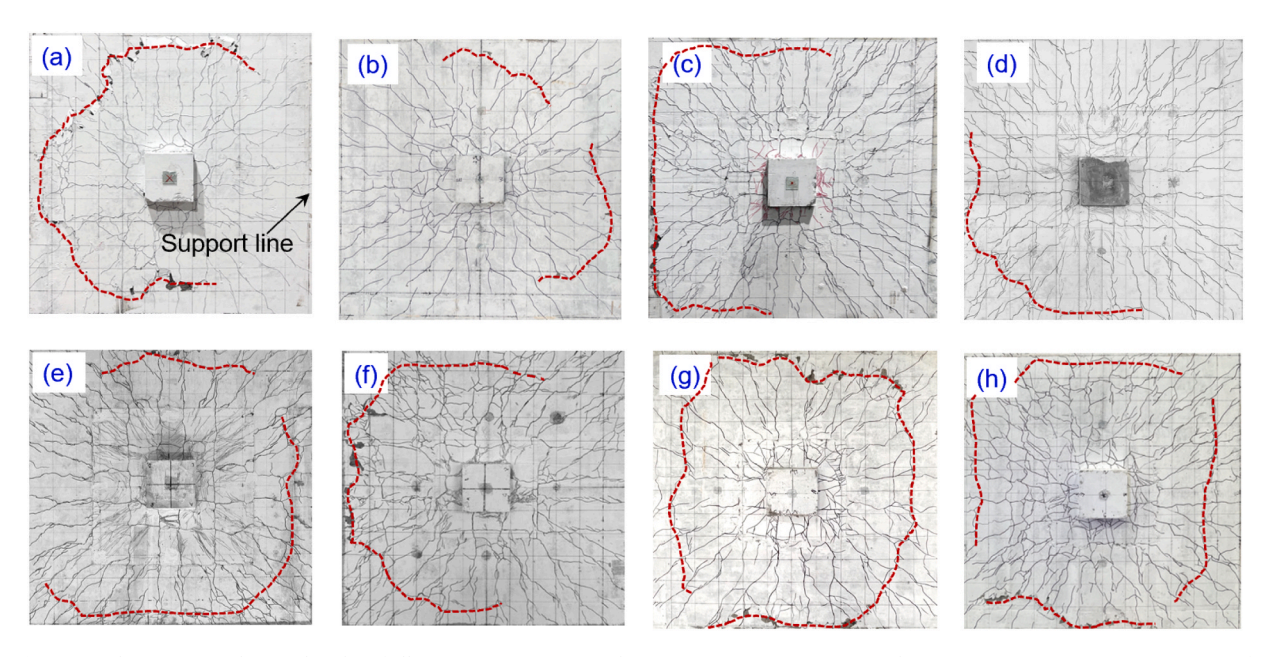


Fig. 6. Crack patterns on the tensile sides of all specimens: (a) NC-1.0, (b) NC-1.5, (c) EC-1.0-PE2-440, (d) EC-1.0-PE2-560, (e) EC-1.0-PE2-680, (f) EC-1.0-SP2-440, (g) EC-1.0-PE1-440, and (h) EC-1.5-PE1-440.

NC-1.5, failure propagated radially from the column edge, following a punching shear surface toward the tension zone of the slab. The punching shear angles of specimen NC-1.0 were measured at 22° on the left side and 21° on the right side. In contrast, specimen with higher reinforcement ratios led to a more pronounced shear failure plane, with measured angles of 26° and 29° . The higher bending and shear strength of ECC leads to a larger punching failure surface for specimens reinforced with ECC. As a result, the critical punching shear crack angle increased, ranging from 30° to 50° .

3.2. Load-deflection responses

Fig. 8 presents the load-deflection curves for the slab-column connections. The control specimens NC-1.0 and NC-1.5 exhibited a brittle punching shear failure mode, featured by small deflections and a sudden drop in applied load. In contrast, the employment of ECC in connection led to notable changes in peak states and developed trends. Connections enhanced with ECC exhibited large deformations and a more ductile response, indicative of a flexural-induced punching shear failure mode. This can be explained by the fact that crack propagation can be effectively suppressed due to the high tensile strain capacity of ECC, resulting in a failure mode predominantly governed by flexural behaviour rather than by sudden punching shear failure. The employment of ECC led to a rise of crack load by 18.58–33.31 % relative to RC connections. The pre-crack stiffness and post-crack stiffness of specimens strengthened with ECC were higher the reference specimen NC-1.0.

3.2.1. Effect of reinforcement ratio

Fig. 9a shows the effect of reinforcement ratio on the load-deflection behaviour of RC connections by comparing specimen NC-1.0 (1.0 % reinforcement ratio) with specimen NC-1.5 (1.5 % reinforcement ratio). Increasing reinforcement ratio had a minimal effect on the pre-cracking stiffness, as first crack behaviour was predominantly governed by the normal concrete's tensile strength. In contrast, the increase of reinforcement ratio significantly improved the post-cracking stiffness of RC connections, which can be primarily ascribed to the role of steel bars during the elastic-plastic stage, and a higher steel reinforcement ratio enhances the tensile resistance, mitigates crack propagation and improves the stiffness of the connections. Consequently, specimen NC-1.5 had smaller deformations than the specimen with a lower reinforcement ratio, due to its similar peak load but higher post-crack stiffness.

Fig. 9b presents the effect of reinforcement ratio on the load-deflection behaviour of connections enhanced with ECC. The reinforcement ratios of EC-1.0-PE1-440 and EC-1.5-PE1-440 were 1.0 % and 1.5 %, respectively. Specimen EC-1.5-PE1-440 exhibited similar pre-crack stiffness but higher post-crack stiffness compared to EC-1.0-PE1-440 as the connections enhanced with ECC had a much better flexural behaviour, and an increased reinforcement ratio further improves its flexural stiffness. The deflection at the peak load for specimen EC-1.5-PE1-440 was 16.19 mm, 22.39 % lower than that of specimen EC-1.0-PE1-440, ascribed to the ductile flexural-induced punching shear failure mode of connections strengthened with ECC, where a higher reinforcement ratio increased susceptibility to punching shear failure, leading to smaller deformations.

3.2.2. Effect of ECC zone area

Fig. 10 shows the effect of ECC zone area on the load-deflection behaviour by comparing specimen EC-1.0-PE2-440 with specimen

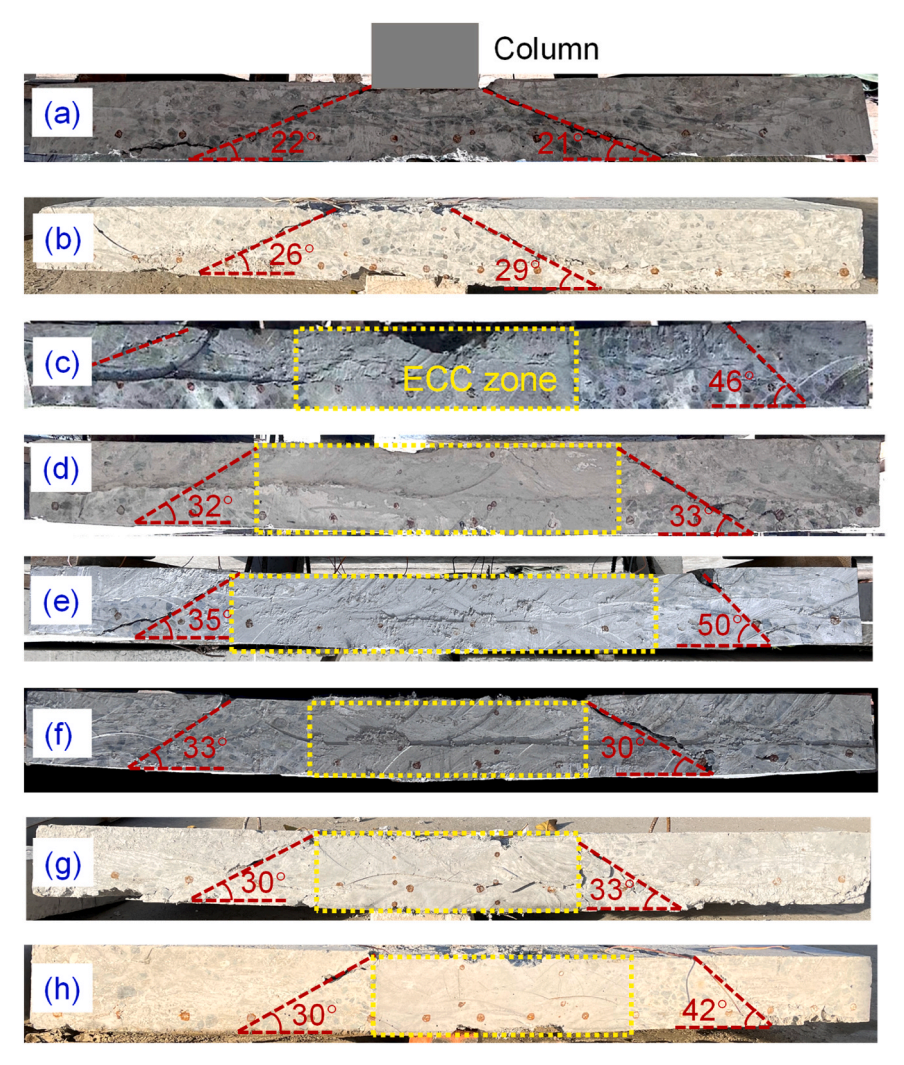


Fig. 7. Saw-cut cross-sections of all specimens: (a) NC-1.0, (b) NC-1.5, (c) EC-1.0-PE2-440, (d) EC-1.0-PE2-560, (e) EC-1.0-PE2-680, (f) EC-1.0-SP2-440, (g) EC-1.0-PE1-440, and (h) EC-1.5-PE1-440.

EC-1.0-PE2–560 and specimen EC-1.0-PE2–680, which contained an ECC zone with a side length of 440, 560 and 680 mm, respectively. The load-deflection curves of connections with ECC experienced a ductile manner with deformation exceeding 20 mm, maybe due to the contribution of ECC in core area that can bear external loads together with rebars. The increase in ECC zone side length from 440 mm to 560 mm and 680 mm had no significant influence on the pre-crack stiffness of specimens, as all specimens exhibited similar crack load behaviour. However, the post-crack stiffness of EC-1.0-PE2–560 was slightly lower than that of EC-1.0-PE2–440 and EC-1.0-PE2–680. This discrepancy can be ascribed to a temporary drop in hydraulic pressure at 200 kN during the test of EC-1.0-PE2–560, which resulted in a brief loss of load control and a slight reduction in the measured stiffness.

3.2.3. Effects of fibre type and dosage in ECC

Fig. 11 illustrates the effects of fibre type and dosage in ECC on the load-deflection behaviour by comparing specimen EC-1.0-PE2–440 (with 2.0 % PE fibre), specimen EC-1.0-SP2–440 (with 0.5 % steel fibre and 1.5 % PE fibre) and specimen EC-1.0-PE1–440 (with 1.0 % PE fibre), which had the same reinforcement ratio and ECC zone area. The load-deflection curves of all specimens exhibited ductile behaviour, confirming the beneficial influence of ECC in enhancing structural performance. The deflection under the ultimate load of specimen EC-1.0-PE1–440 was 20.86 mm, 12.24 % and 8.31 % lower than that of specimens EC-1.0-PE2–440 and EC-1.0-SP2–440, indicating that the increase of fibre dosage from 1 % to 2 % in ECC could effectively improve the deformation capacity of the connections. Among them, specimen EC-1.0-SP2–440 exhibited the highest pre-crack and post-crack stiffness, followed by specimen EC-1.0-PE2–440, while specimen EC-1.0-PE1–440 had the lowest stiffness. It suggests that incorporating steel fibre in ECC can contribute to enhanced stiffness both before and after cracking. Compared to specimen EC-1.0-PE1–440 (with 1 % fibre), the pre-crack stiffness and post-crack stiffness of EC-1.0-PE2–440 (with 2.0 % fibre) were higher, which can be attributed to the enhanced tensile properties of ECC with a higher fibre dosage, as seen in Fig. 1, leading to a significantly enhanced deformation and stiffness resistance.

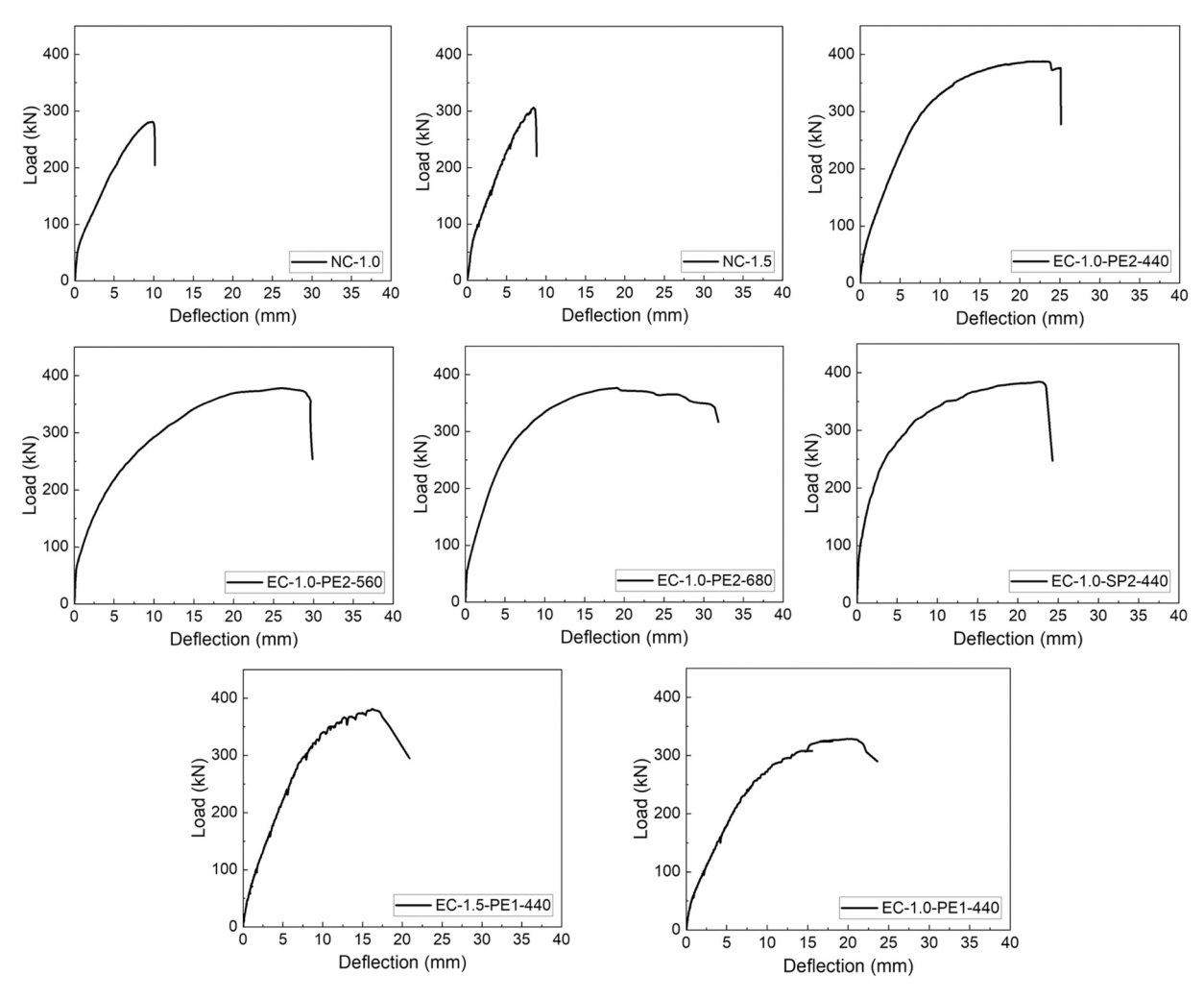


Fig. 8. Load-deflection curves of all specimens.

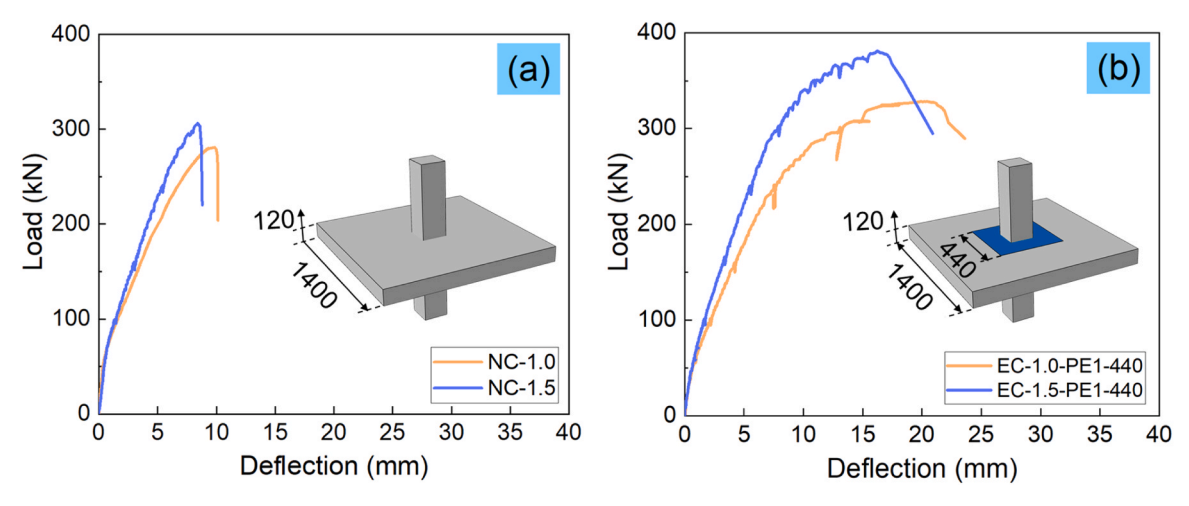


Fig. 9. Load-deflection curves of connections with different reinforcement ratios: (a) RC connections, and (b) RC connections enhanced with ECC.

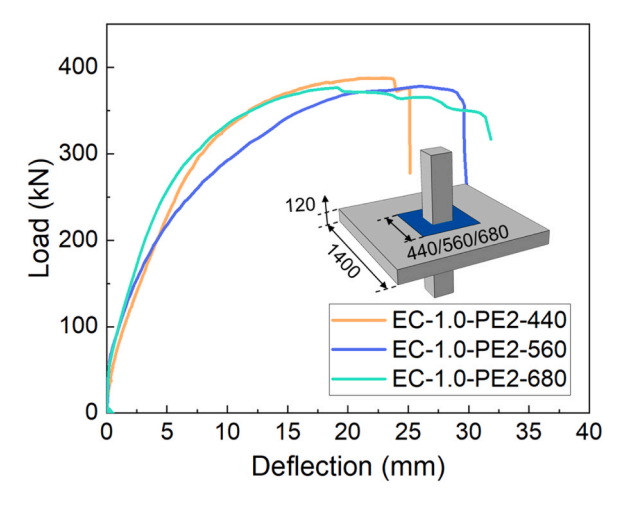


Fig. 10. Load-deflection curves of connections with different ECC zone areas.

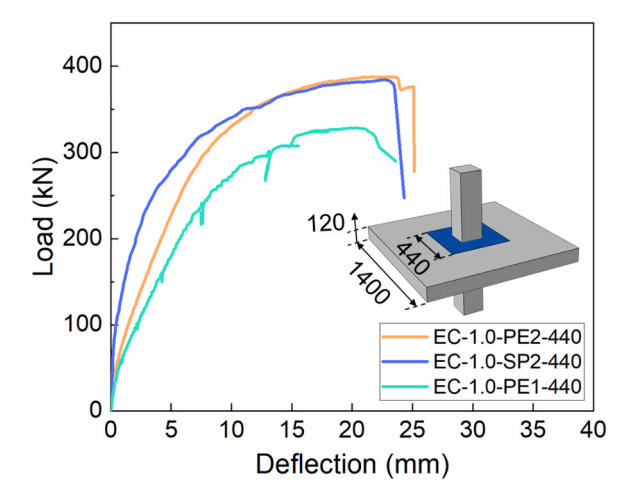


Fig. 11. Load-deflection curves of connections with ECC containing different fibre types and dosages.

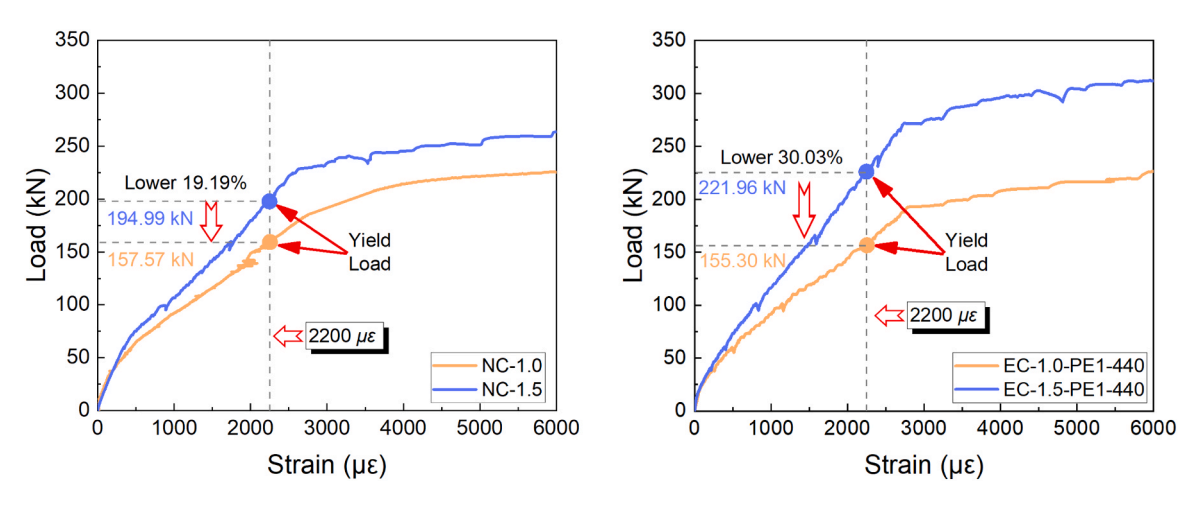


Fig. 12. Load-strain curves of connections with different steel reinforcement ratios: (a) RC connections, and (b) RC connections enhanced with ECC.

3.3. Load-strain responses

Herein, the strains of steel reinforcement were evaluated under varying parameters, with strain data obtained as the average of two readings recorded at the locations illustrated in Fig. 4c. The yield strain of steel reinforcement was determined as 2200 $\mu\varepsilon$.

3.3.1. Effect of steel reinforcement ratio

Fig. 12a displays the load-strain curves of steel rebars in RC connections with varying steel reinforcement ratios. The strain of steel reinforcement exceeded 2200 $\mu\epsilon$, indicating that steel reinforcement yielded in RC connections. Under the same load, specimen NC-1.0 exhibited a higher steel strain relative to specimen NC-1.5, suggesting that in connection with a lower steel reinforcement ratio, the steel rebars carry a larger proportion of the applied load, resulting in increased strain under the same external force. The load corresponding to yield point of specimen NC-1.0 was 157.57 kN, which was 19.19 % lower than its counterpart with a steel reinforcement ratio of 1.5 %, implying that connections with a higher steel reinforcement could bear greater external force before reaching yield.

Fig. 12b shows the load-strain curves of steel rebars in connections with ECC at different steel reinforcement ratios. A similar trend was observed, where connections with a higher reinforcement ratio exhibited lower steel reinforcement strain under the same applied load. The load at the yield point of specimen EC-1.0-PE1-440 was 155.3 kN, 30.03 % lower than that of specimen EC-1.5-PE1-440 with the load of 221.96 kN. In connections with ECC, the drop in steel strain and the rise in yield load due to a higher reinforcement ratio were more pronounced against RC connections. This is primarily because RC connections typically exhibit brittle punching shear failure, where the role of steel reinforcement is relatively limited. In contrast, connections with ECC tended to follow a flexural-induced punching shear failure, making the reinforcement ratio a more significant factor in determining the overall mechanical performance.

3.3.2. Effect of ECC zone area

Fig. 13 demonstrates the load-strain curves of steel rebars in connections with varying ECC zone areas. The loads corresponding to yield point of specimens EC-1.0-PE2-440, EC-1.0-PE2-560 and EC-1.0-PE2-680 were 200.75, 202.77, and 232.5 kN, respectively. A larger ECC zone provided a broader area to resist compressive forces, further improving the yield load capacity of the connections.

3.3.3. Effects of fibre type and dosage in ECC

Fig. 14 presents the load-strain curves of steel rebars in connections with different fibre types and dosages in ECC. Under the same load, specimen EC-1.0-PE1–440 exhibited the largest strain in steel reinforcement, while specimens EC-1.0-PE2–440 and EC-1.0-SP2–440 had the similar value prior the yield point. The load corresponding to yield point of specimens EC-1.0-PE2–440, EC-1.0-SP2–440 and EC-1.0-PE1–440 were 200.75, 211.49, and 155.3 kN, respectively. The fibre type in ECC with dosage of 2 % had a minimal impact on the load transfer in connections. It is because the addition of steel fibre improved the elastic modulus and crack-bridging efficiency in shear stress transfer across microcracks, while simultaneously imposing a reduction in tensile ductility. A higher fibre dosage improved crack control and energy dissipation, reducing localised strain on the steel reinforcement and increasing the yield load.

3.4. Load-bearing capacity

3.4.1. Effect of steel reinforcement ratio

Fig. 15a illustrates a comparison of the crack and peak loads of RC connections with different steel reinforcement ratios. Specimen NC-1.0 had a crack load of 46.77 kN and a peak load of 306.42 kN, performing similarly to specimen NC-1.5, indicating that increasing reinforcement ratios had a little effect on the bearing capacity of RC connection, governed by a brittle punching shear failure mode. In

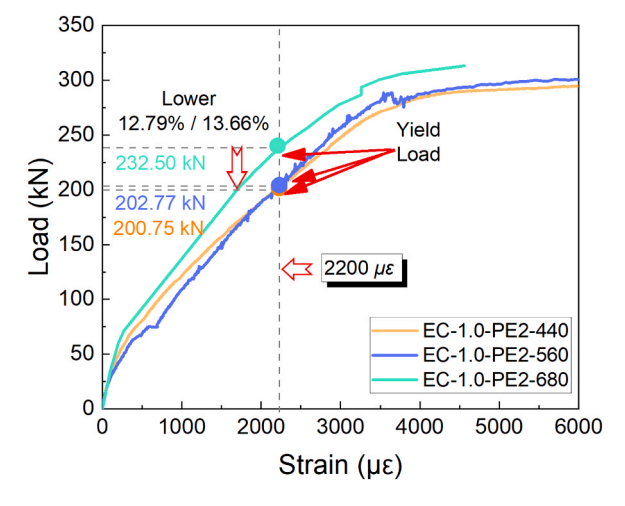


Fig. 13. Load-strain curves of connections with different ECC zone areas.

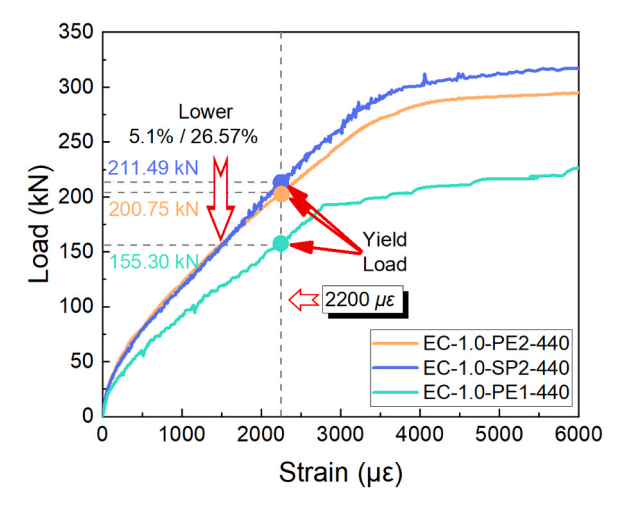


Fig. 14. Load-strain curves of connections with ECC containing different fibre types and dosages.

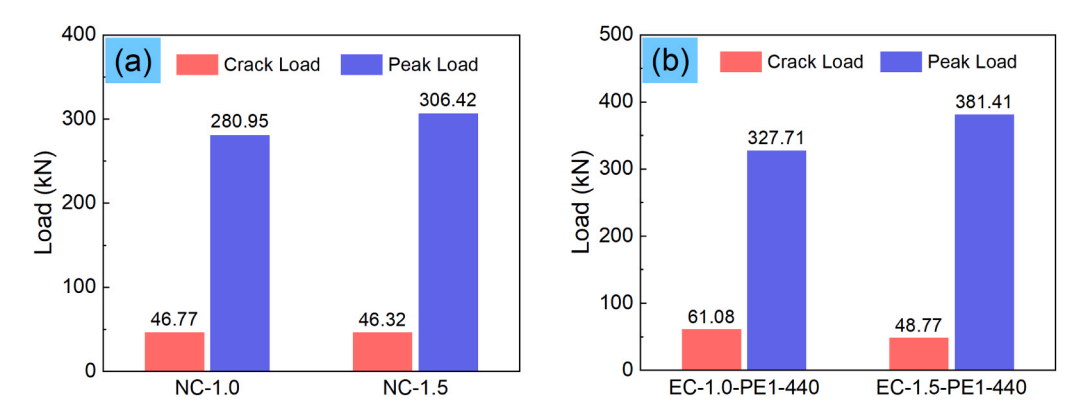


Fig. 15. Crack and peak loads of connections with different steel reinforcement ratios.

conclusion, under punching shear-controlled failure, increasing the steel reinforcement ratio did not obviously enhance the load-bearing performance of RC connections.

Fig. 15b shows the crack and peak loads of RC connections enhanced with ECC with different steel reinforcement ratios. Increasing the reinforcement ratio contributed to an increase in peak load for connections enhanced with ECC. Specimen EC-1.5-PE1–440 achieved a peak load of 381.41 kN, 16.39 % higher than that of specimen EC-1.0-PE1–440, attributed to the failure mode of connections with ECC featured by flexural-induced punching shear failure mode.

3.4.2. Effect of ECC zone area

Fig. 16 shows the crack and peak loads of RC specimens enhanced with ECC with varying ECC zone areas. The crack loads of specimens EC-1.0-PE2-440, EC-1.0-PE2-560 and EC-1.0-PE2-680 were 55.48, 60.01, and 62.35 kN, respectively. It indicates that a larger ECC zone area exhibited an improvement of crack load for connections. In terms of peak load, an increase ECC zone area resulted in a slight decrease in connections with ECC, as the punching shear cone formed the concrete region and the failure of connection was mainly governed by the normal concrete strength. In conclusion, the side length ECC zone at distance equal to 1.0 times the slab thickness from the column face would be the better choice.

3.4.3. Effects of fibre type and dosage in ECC

Fig. 17 presents the crack and peak loads of RC specimens enhanced with ECC, containing different fibre types and dosages. Specimen EC-1.0-PE2-440, with a higher fibre dosage, outperformed its counterpart of specimen EC-1.0-PE1-440, improving the connection's crack load and peak load by 4.36 % and 17.20 %, respectively. It suggests that a higher fibre dosage can more effectively enhance the bridging effect, delaying crack propagation and thereby improving the tensile resistance and crack control of the connections. Specimen EC-1.0-SP2-440 had the largest crack load among these connections, implying that incorporating an appropriate amount of steel fibres is more beneficial for enhancing the crack resistance of the connection compared to solely increasing the PE fibre content (2.0 %). However, partially replacing PE fibres with steel fibres in ECC did not seem to affect the punching shear resistance of connection, where specimen EC-1.0-PE2-440 had a peak load of 384.07 kN and specimen EC-1.0-SP2-440 had a peak load of

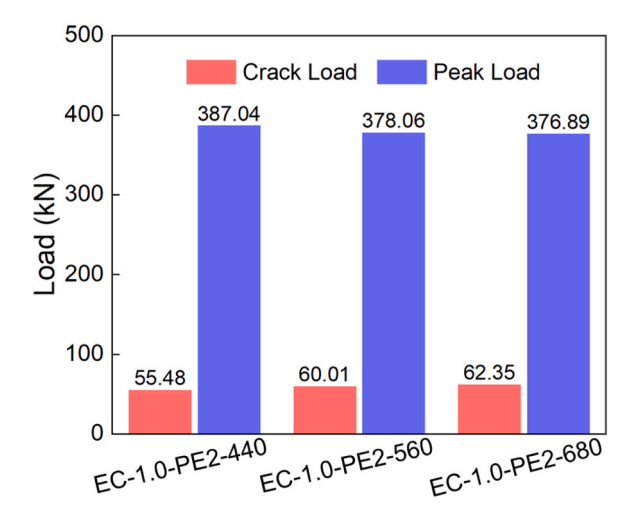


Fig. 16. Crack and peak loads of specimens with different ECC zone areas.

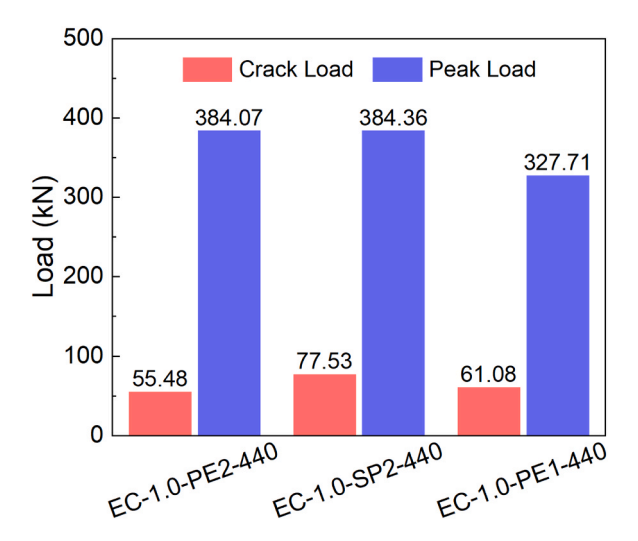


Fig. 17. Crack and peak loads of connections with ECC containing different fibre types and dosages.

384.36 kN.

4. Theoretical analysis

4.1. Characteristics of the failure zone

The critical punching shear perimeter is a critical parameter in predicting the punching shear resistance of slab-column connections. According to current design codes, e.g., GB50010–2010 [35] and ACI 318–19 [37], the coefficient k that affects the determination of u_0 is taken as 0.5 for normal RC connections. However, experimental observations revealed that the punching shear failure surface did not initiate entirely from the column edge, and the bottom perimeter of the punching cone was notably expanded in connections strengthened with ECC. This may be attributed to the inclusion of ECC, which altered the load transfer mechanism and improved the flexural performance of the connection. As a result, the traditional definition of the critical punching shear perimeter cannot be entirely applicable when ECC was used. To account for the enlarged failure surface and the corresponding increase in the effective loading area, the critical punching shear perimeter should be modified to accurately evaluate the punching shear resistance of connections incorporating ECC. Consequently, the revised critical punching shear perimeter u_0 is calculated as:

$$u_0 = 4(c + 2kh_0)\#$$
 (1)

$$k = \frac{\pi(r_t + r_b) - 4c}{8h_0} \#$$
 (2)

where u_0 is the critical punching shear perimeter, c represents the side length of the ECC zone for ECC-strengthened connections or the column side length for RC connections, k is the coefficient where the position of the critical section from the edge of the column, h_0 is the effective depth of the slab, and r_t and r_b are the average radius of the failure punching cone at the top and bottom sides of the tested slabs, respectively. When the punching shear crack initiated at either the column edge or the ECC edge, the values of c and r_t were identical.

Figs. 18 and 19 shows the relationship between the ratio of c to h_0 and coefficient k in connections with ECC. Through regression fitting, the relationship between c/h_0 and coefficient k can be expressed as $k = -0.254(\frac{c}{h_0}) + 2.22$, with a R^2 value of 0.96. Moreover, the linear regression yielded a small standard deviation of 0.0055 for this model, indicating high parameter stability.

4.2. Comparison with design codes and yield line theory

Five existing code provisions are summarised in Table 6 to compare their predictions with the modified coefficient k to evaluate their applicability for estimating the punching shear strength of RC specimens with ECC. The value of c was also adjusted to be the side length of ECC zone considering the critical sections of the punching shear cones outside the ECC zone. Flexural strength evaluation of ECC-enhanced connections was conducted using yield line theory, which has been derived and presented in a previous study [34].

Table 7 displays the experimentally measured punching shear resistance (V_{EXP}) and theoretical predictions obtained from existing code designs after applying the modified coefficient k and yield line theory. The average ratio of experimental to theoretical strength along with the corresponding CoV were calculated to provide insights into the accuracy and consistency of these predictions. It can be seen that all predicted resistance based on existing code designs exhibited a small CoV, implying that the predictions are relatively consistent and reliable across different design approaches, with low variability in the estimated punching shear capacities. The modified GB50010–2010 [29] yielded an average ratio of 1.04 with a CoV of 6.30 %, suggesting a good agreement with the experimental data for connections enhanced with ECC. In contrast, the modified ACI 318–19 [37] and FIB codes [38] led to average ratios of 0.91 (CoV=6.35 %) and 0.86 (CoV=7.90 %), indicating that these provisions tended to underestimate the punching shear resistance. Meanwhile, the modified DIN 1045–1 [39] provision showed a good agreement with experimental results. However, EC2 provision [40] significantly overestimated the punching shear resistance when the proposed coefficient k was used. Moreover, the estimated flexural strengths based on the yield line theory are generally higher than experimental data, as the theory represents the ultimate limit state of the member, assuming a fully plastic distribution of internal forces, assuming a fully plastic internal force distribution [41].

Fig. 20 illustrates the effect of ECC side length variation on the punching shear resistance predictions based on the existing design codes. Most design codes except EC2 accurately estimated the punching shear resistance for connections with an ECC side length of 440 mm, maintaining an error margin within 15 %. It should be noted that the predictions for specimen EC-1.0-PE1-440 based on ACI and FIB codes exceeded the 15 % error range. This suggests that a reduction of fibre dosage has a significant adverse effect on the punching shear resistance of connections, although the failure surface formed outside the ECC zone, and its influence should be further considered by introducing an appropriated factor. When the ECC side length was 560 mm ad 680 mm, corresponding to distances of 1.5 and 2.0 times the slab thickness from the column edge, the predictions based on GB 50010-2010, ACI and DIN 1045-1 showed good agreement with the experimental results. In contrast, EC2 consistently underestimated the punching shear resistance, while FIB code tended to overestimate it.

GB50010–2010 [35] and DIN 1045–1 [39] provided reliable estimate for connections enhanced with ECC after modification. Further revisions of design codes should consider both dimension of ECC zone and material-specific parameters (e.g., fibre dosage) to improve the accuracy of predictions for connections enhanced with ECC.

5. Conclusions

In this study, the punching shear behaviour of RC connections enhanced with ECC accounting for the effects of steel reinforcement

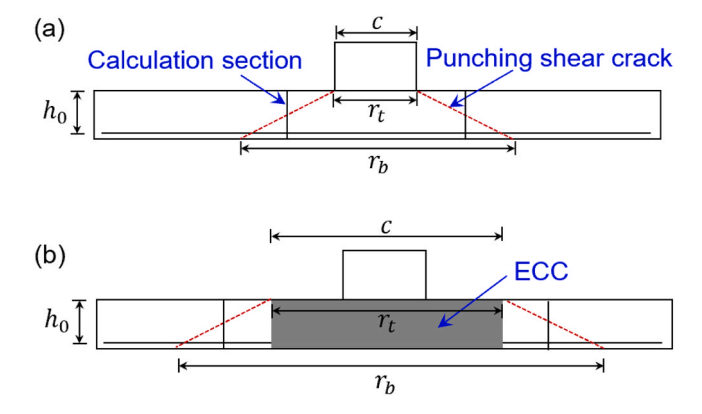


Fig. 18. Schematic diagram for calculating the punching shear capacity of the slab.

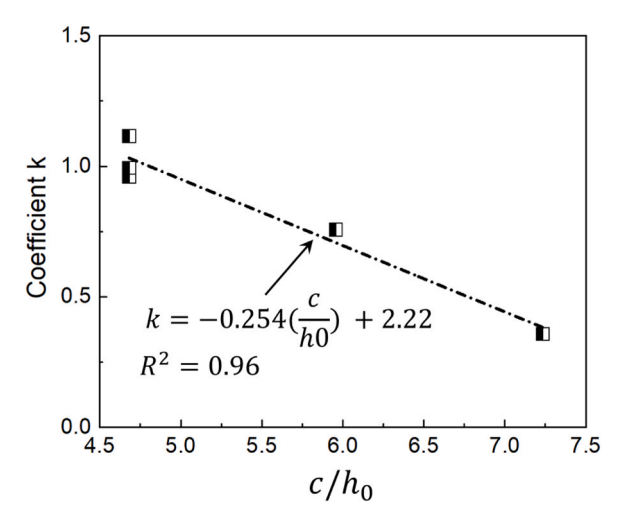


Fig. 19. Fitting curve between coefficient k and c/h_0 for connections with ECC.

Table 6Summary of code provisions for predicting the punching shear strength.

Ref.	Equations	Critical perimeter
GB 50010–2010	$egin{align} V_p &= 0.7 eta_h f_i \eta u_0 h_0 \ \eta_1 &= \min(0.4 + rac{1.2}{eta}, \ 0.5 + rac{lpha_s h_0}{4u}) \ \end{array}$	$u_0 = 4(c + h_0)$ $k = 0.5$
ACI 318-19	$V_p = \min[0.33\sqrt{f_c}u_mh_0, (0.17 + \frac{0.083a_sh_0}{u_m})\sqrt{f_c}u_mh_0, (0.17 + \frac{0.33}{\beta_s})\sqrt{f_c}u_mh_0]$	$u_0 = 4(c + h_0)$ $k = 0.5$
DIN 1045-1	$V_p = 0.21(1+\sqrt{rac{200}{h_0}})(100 ho f_c)^{rac{1}{3}}u_m h_0$	$u_0 = 4c + 3\pi h_0$ $k = 1.5$
	$1+\sqrt{rac{200}{h_0}} \leq 2.0 \; \sqrt{ ho_{x} ho_{y}} < 0.4f_c/f_y < 0.02$	
EC2	$V_P=rac{0.18}{\gamma}K(100 ho f_c^{\prime})^{rac{1}{3}}u_mh_0$	$u_0 = 4(c + \pi h_0)$ k = 2.0
	$ ext{K=}1+\sqrt{rac{200}{h_0}}\leq 2.0\sqrt{ ho_x ho_y}<0.02$	
FIB	$V_p = K_{\psi} \sqrt{f_c} u_m h_0$	$u_0 = 4(c + h_0)$ $k = 0.5$
	$K_{\psi} = \frac{1}{1.5 + 0.9 \psi dk_{dg}} \le 0.6$	
	$k_{ m dg} = rac{32}{16+d_{ m g}} \geq 0.75$	
	$\psi = 1.5 r_{\rm s} \frac{f_{\rm y}}{h_0 E_{\rm S}}$	

Note: β_h : the height effect coefficient, 1.0 if $h \le 800$ mm; 0.9 if $h \ge 2000$ mm; f_i : concrete axial tensile strength; β_s : ratio of long side to short side of column, $2 \le \beta_s < 4$; α_s : 40 for interior columns, 30 for edge columns, and 20 for corner column; f_c : concrete cylinder compressive strength; ρ_x and ρ_y relate to the bonded tension steel in x- and y- directions, respectively; K_{ψ} : parameter accounting for the effect of the width of the critical shear; k_{dg} : factor accounting for the effect of the aggregate size; ψ : slab rotation; E_s : Young's modulus of the flexural reinforcement; r_s : distance between the centroid of the loaded area to the line of zero radial bending moments (line of contraflexure); d_g : the maximum aggregate size.

Table 7
Comparison of experimental and theoretical results for connections with ECC.

Specimen ID	V_{EXP}/V_{GB}	V_{EXP}/V_{ACI}	V_{EXP}/V_{DIN}	V_{EXP}/V_{EC2}	V_{EXP}/V_{FIB}	V_{EXP}/V_{YLT}
EC-1.0-PE2-440	1.11	0.97	1.21	1.41	0.93	0.92
EC-1.0-PE2-560	1.03	0.90	1.08	1.26	0.83	0.90
EC-1.0-PE2-680	0.98	0.85	0.99	1.16	0.76	0.93
EC-1.0-SP2-440	1.11	0.99	1.20	1.40	0.92	0.96
EC-1.0-PE1-440	0.94	0.84	1.02	1.19	0.79	0.89
EC-1.5-PE1-440	1.10	0.98	1.04	1.21	0.91	0.80
AVERAGE	1.045	0.922	1.09	1.272	0.857	0.900
CoV	6.41 %	6.67 %	7.85 %	7.78 %	7.79 %	5.56 %

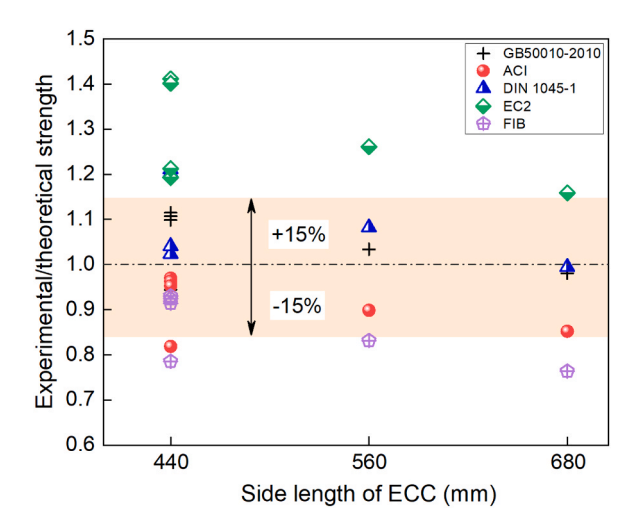


Fig. 20. A comparison between the experimental and predicted strengths of connections with ECC.

ratio, ECC zone area, and fibre type and dosage in ECC was investigated. The main conclusions are summarized as follows:

- (1) Incorporating ECC into the connection zone could effectively improve the load-carry bearing capacity and modify the failure response from punching shear mode to flexural-punching shear failure mode. An optimal ECC zone was achieved with a side length equal to the slab thickness, offering a good balance between performance enhancement and economic cost.
- (2) An increased reinforcement ratio had a little effect on the punching shear resistance of RC connections which were governed by brittle punching shear failure, but resulted in a higher peak load and post-crack stiffness in connections enhanced with ECC due to the flexural-induced punching shear failure mechanism. In all specimens, the reinforcing bars reached their yield point. Connections with a higher steel reinforcement could bear greater external force before reaching yield.
- (3) The connections with a higher PE fibre dosage had a 17.20 % higher peak load and a 29.27 % higher yield load compared to its counterpart with 1 % fibre dosage, while incorporating steel fibre into ECC improved the crack resistance and stiffness of the connections but did not affect the punching shear resistance and yield load.
- (4) The connections enhanced with ECC exhibited an enlarged punching shear failure surface because of the higher flexural and shear strengths of ECC, which effectively increased the loading area. The angle of punching shear cone increased ranging from 30° to 50° .
- (5) The estimated flexural strengths based on the yield line theory are generally higher than experimental results, as the yield line theory provides an upper-limit solution. The design codes, GB50010–2010 and DIN, provided reliable estimates for connections featuring an ECC-based outer critical section of the punching shear cone after modification.

Given the limited data, additional experiments are needed to refine and validate the critical perimeter of connections enhanced with ECC. Moreover, numerical simulations are required to systematically investigate the influences of various parameters on the punching shear behaviour of connections, providing more robust theoretical support for engineering applications. These are subjects of ongoing research, which will be presented in future publications.

CRediT authorship contribution statement

Xinru Wang: Investigation, Formal analysis. Mingwen Xu: Writing – review & editing, Investigation. Chang Wu: Writing – review & editing, Supervision, Resources, Project administration, Funding acquisition, Conceptualization. Yanli Su: Writing – original draft, Methodology, Investigation, Data curation. Mingzhong Zhang: Writing – review & editing, Supervision. Chenhua Jin: Conceptualization.

Declaration of Competing Interest

The authors declare that they have no known competing financial interests or personal relationships that could have appeared to influence the work reported in this paper.

Acknowledgements

The research presented in this paper were sponsored by the National Natural Science Foundation of China (Grant Nos: 52108119, 52478146), Postgraduate Research & Practice Innovation Program of Jiangsu Province (Grant No.: KYCX23_0283) and SEU Innovation Capability Enhancement Plan for Doctoral Students (Grant No.: CXJH_SEU24090).

Data availability

Data will be made available on request.

References

- [1] R.P. Manfredi, F.D.A. Silva, D.C.T. Cardoso, On punching shear strength of steel fiber-reinforced concrete slabs-on-ground, Acids Struct. J. 119 (4) (2022) 185–196
- [2] Marcos D.E. Teixeira, Joaquim A.O. Barros, Vítor M.C.F. Cunha, Bernardo N. Moraes-Neto, António VG. Numerical simulation of the punching shear behaviour of self-compacting fibre reinforced flat slabs, Constr. Build. Mater. 74 (15) (2015) 25–36.
- [3] R. Koppitz, A. Kenel, T. Keller, Punching shear of RC flat slabs review of analytical models for new and strengthening of existing slabs, Eng. Struct. 52 (2013) 123–130.
- [4] I.G. Shaaban, H.A. Hosni, M.W. Montaser, M.M. El-Sayed, Effect of premature loading on punching resistance of reinforced concrete flat slabs, Case Stud. Constr. Mat. 12 (2020) e00320.
- [5] Y.Z. Yang, M.Z. Diao, Y. Li, H. Guan, X.Z. Lu, Post-punching failure mechanism and resistance of flat plate-column joints with in-plane constraints, Eng. Fail Anal. 138 (2022) 106360.
- [6] S. Garg, V. Agrawal, R. Nagar, Case study on strengthening methods for progressive collapse resistance of RC flat slab buildings, Structures 29 (2021) 1709–1722.
- [7] S. Garg, V. Agrawal, R. Nagar, Progressive collapse behaviour of reinforced concrete flat slab buildings subject to column failures in different storeys, Mater. Today. Proc. 42 (2) (2021) 1031–1037.
- [8] W.J. Yi, F.Z. Zhang, S.K. Kunnath, Progressive collapse performance of RC flat plate frame structures, J. Struct. Eng. 140 (9) (2014) 04014048.
- [9] B. Ye, P. Pan, G. Xiao, Y. Zhang, Z. He, Experimental investigation on failure modes of RECC slab-column connections under concentric gravity loading, Eng. Struct. 230 (2021) 111559.
- [10] M. Elsayed, I. Abdel-Hady, L.M. Abdel-Hafez, Y.R. Tawfic, Strengthening of slab-column connections using ultra high-performance fiber concrete, Case Stud. Constr. Mat. 17 (2022) e01710.
- [11] A. Said, M. Elsayed, A.A. El-Azim, F. Althoey, B.A. Tayeh, Using ultra-high performance fiber reinforced concrete in improvement shear strength of reinforced concrete beams, Case Stud. Constr. Mat. 16 (2022) e01009.
- [12] K. Zhou, J.A. Qi, J.Q. Wang, Post-cracking punching shear behavior of concrete flat slabs partially reinforced with full-depth UHPC: experiment and mechanical model, Eng. Struct. 275 (2023) 115313.
- [13] Y. Zhou, H.W. Shou, C. Li, Y.B. Jiang, X. Tian, Punching shear behavior of ultra-high-performance fiber-reinforced concrete and normal strength concrete composite flat slabs, Eng. Struct. 322 (2025) 119123.
- [14] V.C. Li, K.Y. Christopher, Steady-state and multiple cracking of short random fiber composites, J. Eng. Mech. ASCE 118 (11) (1992) 2246-2264.
- [15] V.C. Li, H. Stang, H. Krenchel, Micromechanics of crack bridging in fiber reinforced concrete, J. Mater. Struct. 26 (162) (1993) 486-494.
- [16] B.T. Huang, K.F. Weng, J.X. Zhu, Y. Xiang, J.G. Dai, Victor Li, Engineered/strain-hardening cementitious composites (ECC/SHCC) with an ultra-high compressive strength over 210 MPa, Compos Commun. 26 (2021) 100775.
- [17] B.T. Huang, J.X. Zhu, K.F. Weng, Victor Li, J.G. Dai, Ultra-high-strength engineered/strain-hardening cementitious composites (ECC/SHCC): material design and effect of fiber hybridization, Cem. Concr. Comp. 129 (2022) 104464.
- [18] P. Zhang, Y.L. Su, Y. Liu, D.Y. Gao, S.A. Sheikh, Flexural behavior of GFRP reinforced concrete beams with CFRP grid-reinforced ECC stay-in-place formworks, Compos Struct. 277 (2021) 114653.
- [19] L.Z. Li, Y. Bai, K.Q. Yu, J.T. Yu, Z.D. Lu, Reinforced high-strength engineered cementitious composite (ECC) columns under eccentric compression: experiment and theoretical model, Eng. Struct. 198 (1) (2019) 109541.
- [20] L.H. Wang, W.H. Shi, L.P. Qian, Y.L. Bai, S.Z. Liu, Z.Q. Yang, Flexural behaviors of GFRP-reinforced engineered cementitious composite (ECC)-concrete composite beams, Eng. Struct. 322 (2025) 120097.
- [21] P. Zhang, X.Y. Chang, Y. Liu, C. Su, S.H. Fan, C. Wu, Z.F. Pan, Experimental study and analytical model of masonry columns confined with fiber grid-reinforced ECC under cyclic compression load, Eng. Struct. 330 (2025) 119560.
- [22] J.Q. Dong, S.S. Zheng, Z.W. Zhang, H. Liu, Y.L. Li, Experimental study on seismic performance of RC beam- CFST column joint combination using ECC, Eng. Struct. 312 (2024) 11888.
- [23] M. Ghalla, M. Badawi, J.W. Hu, G. Elsamak, E.A. Mlybari, M. Emara, Ultimate performance of two-way reinforced concrete flat slabs enhanced by SHCC drop panels mitigating punching failure, J. Build. Eng. 99 (2025) 111574.
- [24] L. Liu, S.S. Yu, X.P. Ma, Flexural capacity of RC beams reinforced with ECC layer and steel plate, J. Build. Eng. 65 (2023) 105781.
- [25] Y.L. Su, X.R. Wang, C. Wu, M.W. Xu, C.H. Jin, Experimental investigation of flexural and punching behavior for plain PE-ECC slabs with different fiber volume fractions and span-depth ratios, Constr. Build. Mater. 441 (2024) 137502.
- [26] B.B. Ye, P. Pan, G.Q. Xiao, J.G. Han, Y.T. Zhang, Comparative study of reinforced-engineered cementitious composites and reinforced-concrete slab-column connections under a vertical monotonic load, Eng. Struct. 244 (2021) 112740.
- [27] B.B. Ye, P. Pan, G.Q. Xiao, Y.T. Zhang, Z. He, Experimental investigation on failure modes of RECC slab-column connections under concentric gravity loading, Eng. Struct. 230 (2021) 111559.
- [28] X.N. Huang, Q.H. Li, J.Z. Tong, S.L. Xu, Y.C. Lu, Punching shear behavior and strength prediction of UHTCC-enhanced RC slab-column joints, Eng. Struct. 286 (2023) 116162.
- [29] X.N. Huang, J.Z. Tong, Q.H. Li, S.L. Xu, Numerical and analytical investigations on punching shear performance of UHTCC-enhanced RC slab-column joints, J. Build. Eng. 79 (2023) 107900.
- [30] Y. Mohammad, A. Taheri, S.M. Zahrai, Punching shear behavior of flat slabs composed of normal concrete and ECC under the unbalanced moment, Struct. Concr. 17 (6) (2016) 959–971.
- [31] Z.X. Yu, G.S. Tong, J.Z. Tong, X.N. Huang, Q.H. Li, S.L. Xu, Punching shear tests and design of UHTCC-enhanced RC slab-column joints with shear reinforcements, Mag. Concr. Res 76 (19) (2024) 1106–1120.
- [32] A. Hamoda, A.A. Abadel, M. Ahmen, V. Wang, Z. Vrcelj, Q.Q. Liang, Punching shear performance of reinforced concrete slab-to-steel column connections incorporating ECC and UHPECC, Eng. Struct. 322 (2025) 119145.
- [33] X.F. Deng, D.Q. Lan, Y.H. Weng, G.L. Chen, K. Qian, Study on punching shear resistance of slab-column connections with partial ECC replacement, Eng. Mech. (2023).
- [34] Y.L. Su, X.R. Wang, C. Wu, M.W. Xu, L. Ma, C.H. Jin, Punching shear behavior of RC slab-column connections enhanced with ECC in core area, Structures 74 (2025) 108567.
- [35] GB 50010-2010, Code for design of concrete structures. Beijing: China Architecture & Building Press, Beijing, 2015.
- [36] JC/T 2416-2018, Test method for mechanical properties of high ductility fiber reinforced cement matrix composites. China Building Materials Industry Press, Beijing, 2018.
- [37] ACI Committee, 2019. ACI 318–19: Building Code Requirements for Structural Concrete and Commentary. American Concrete Institute: Farmington Hills, MI, USA.
- [38] FIB-federation internationale du beton, 2013. fib model code for concrete structures 2010. John Wiley & Sons.

- [39] DIN 1045-1, 2008. German Institute for Standardization Concrete, Reinforced and Prestressed Concrete Structures-Part 1: Design and Construction. [40] CEN (European Committee for Standardization), 2004. Design of concrete structures-Part 1-1: General rules and rules for buildings. Eurocode 2.
- [41] M.W. Bræstrup, Yield-line theory and limit analysis of plates and slabs, Mag. Concr. Res. 22 (71) (1970) 99-106.